

RbIO₃ and RbIO₂F₂: Two Promising Nonlinear Optical Materials in Mid-IR Region and Influence of Partially Replacing Oxygen with Fluorine for Improving Laser Damage Threshold

Qi Wu,^{†,‡} Hongming Liu,[†] Fangchao Jiang,[†] Lei Kang,[§] Lei Yang,[§] Zheshuai Lin,^{*,§} Zhanggui Hu,[§] Xingguo Chen,[†] Xianggao Meng,[⊥] and Jingui Qin^{*,†}

[†]Department of Chemistry, Wuhan University, Wuhan 430072, China

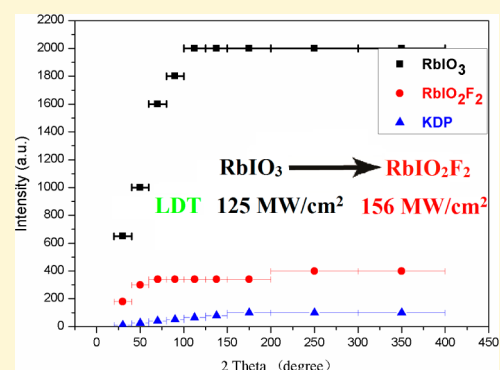
[‡]Department of Chemistry, Hubei Normal University, Huangshi, Hubei 435002, China

[§]Beijing Center for Crystal R&D, Technical Institute of Physics and Chemistry, Chinese Academy of Sciences, Beijing 100190, China

[⊥]College of Chemistry, Central China Normal University, Wuhan 430079, China

S Supporting Information

ABSTRACT: Laser damage threshold (LDT) has been considered as a key index, apart from the nonlinear optical (NLO) effect, to characterize the performance of a mid-infrared NLO material. This paper reports and compares the properties of RbIO₃ and RbIO₂F₂ as potential nonlinear optical (NLO) materials to be used in the mid-IR region. RbIO₃ is a known compound, and its powder SHG (second harmonic generation) effect is carefully measured in this work for the first time to be as strong as 20 times that of KDP, and its powders show a high damage threshold (LDT) of 125 MW/cm². In order to investigate the influence on the properties by partially replacing oxygen with fluorine atoms, the new compound RbIO₂F₂ is synthesized and characterized. Although it also shows relatively strong powder SHG responses 4 times that of KDP, the LDT value of the powders is improved to 156 MW/cm². The transparent region and the thermal stability of two compounds are also measured with satisfactory results. The electronic structure and the properties of the materials are also investigated by the theoretical approach. All these indicate that RbIO₃ and RbIO₂F₂ are both promising candidates for NLO materials to be used in the mid-IR region and that partially replacing oxygen with fluorine in the molecule can improve the laser damage threshold of the material.



INTRODUCTION

For decades, great efforts have been made to explore new nonlinear optical (NLO) materials due to their important applications for laser frequency conversion, optical parameter oscillators (OPOs), signal communication, and so forth,¹ especially in the mid-IR atmospheric window with wavelengths of 3–5 μm. However, the application of currently commercialized NLO crystals in the mid-IR region such as AgGaS₂,² AgGaSe₂,³ and ZnGeP₂⁴ have been heavily limited for their low laser damage threshold (LDT). To search for new mid-IR NLO materials with high LDT and good comprehensive properties has become one of the greatest challenges in this field.^{5–16}

Many metallic iodates compounds have been studied for NLO properties in the IR region for quite a long time.^{17–29} α-LiIO₃ and KIO₃ have been reported to be nonlinear optical materials in the past.^{30,31} RbIO₃ is a known compound whose crystal structure was reported by Alcock with a non-centrosymmetric structure.³² In the literature,³³ it was mentioned that “Powder measurements on a number of iodates such as KIO₃, LiIO₃, TlIO₃, and RbIO₃ have shown that these materials also have large nonlinear coefficients and are phase

matchable.” However, its specific SHG intensity or LDT value has not been reported yet.³⁴ Therefore, we synthesize this compound and systematically measure its SHG (second harmonic generation) effect, LDT, and thermal properties. Moreover, we are especially interested in exploring the Rb–I–O–F system by partially replacing O^{2–} of RbIO₃ with F[–] owing to the fact that the strongest electronegativity of F[–] is helpful to expand the band gap so as to lead to higher LDT. A compound in the Rb–I–O–F system as NLO material has not been investigated. As a result, a new compound RbIO₂F₂ is synthesized by hydrothermal reaction. Indeed, this compound exhibits wider band gap and higher LDT compared with the parent compound RbIO₃ and shows good mid-IR NLO performance. This paper reports the synthesis, crystal structure, optical properties, and the theoretical study of these two compounds. RbIO₃ and RbIO₂F₂ have shown very large SHG effects (20 and 4 times KDP, respectively), high LDT (125 and

Received: November 23, 2015

Revised: February 1, 2016

156 MW/cm²), which is 24 and 30 times that of AgGaS₂ (5.2 MW/cm²) in the same test conditions and wide transparent wavelength regions (up to 13 and 12 μm), with a relatively high thermal stability (550 and 400 °C). The results indicate that RbIO₃ and RbIO₂F₂ are both new candidates for NLO materials in the IR region. More importantly, the compound RbIO₂F₂ obtained by introducing F⁻ into RbIO₃ may open a way for exploring new NLO materials with higher LDT and good comprehensive properties in A–I–O–F systems.

EXPERIMENTAL SECTION

Reagents. All starting materials were commercially available from Sinopharm with analytical grade and used without further treatment.

Synthesis of RbIO₃. RbIO₃ was synthesized by hydrothermal reactions in this work. The mixture of Rb₂CO₃ (1 mmol), HIO₃ (2 mmol), and H₂O (3 mL) in an autoclave equipped with a Teflon liner (23 mL) was heated at 230 °C for 83 h, followed by slow cooling to room temperature at a rate of 1.5 °C/h. The reaction product was washed with cold water and dried in air. A colorless block crystal of RbIO₃ was obtained as single phases (0.4820 g, yield is 93%) (Figure S1).

Synthesis of RbIO₂F₂. RbIO₂F₂ was synthesized by hydrothermal reaction of a mixture of RbIO₃ (3 mmol) and hydrofluoric acid solution (3 mL) in an autoclave equipped with a Teflon liner (23 mL). The mixture was heated at 230 °C for 24 h and then slowly cooled to room temperature at a rate of 3 °C/h. After filtration, the filtrate was slowly volatilized at room temperature. A few days later, large colorless massive crystals were harvested with the different size up to 10 × 10 × 3 mm³ (0.6800 g, yield is 80%) (Figure S2).

Single Crystal Structure Determination. The crystal data collection were performed at 298 (K) using a Bruker SMART APEX diffractometer equipped with a CCD detector using graphite-monochromated Mo Kα (λ = 0.71073 Å) radiation. The transparent single crystals of RbIO₃ and RbIO₂F₂ with dimensions of ca. 0.08 × 0.06 × 0.02 mm³ and 0.06 × 0.05 × 0.02 mm³ were mounted on the glass fiber with epoxy for structure determination. The software package SAINT PLUS³⁵ was used for data set reduction and integration for RbIO₃ and RbIO₂F₂. The crystal structures were solved by direct methods with SHELXS-97 and refined by full-matrix least-squares on F² with SHELXL-97.³⁶ The final refined crystallographic data and structure refinement information are summarized in Table 1. The atomic coordinates and equivalent isotropic displacement parameters are shown in Tables S1 and S2, and some selected important bond lengths and angles are listed in Tables S3–S6 in the Supporting Information. The CCDC numbers for RbIO₃ and RbIO₂F₂ are 1435343 and 1435342, respectively.

Powder X-ray Diffraction. X-ray diffraction patterns of polycrystalline material was obtained at room temperature on Bruker D8 Advanced diffractometer with Cu Kα₁ radiation (λ = 1.54186 Å) in the range of 10–70° at a scanning rate of 0.5°/min. The purities of RbIO₃ and RbIO₂F₂ were confirmed by XRD studies, and the XRD pattern matches the one calculated from single-crystal XRD analysis very well (see Figure S3 and S4).

Energy Dispersive X-ray Spectroscopy (EDS) Measurements. Energy dispersive X-ray spectroscopy (EDS) was performed on a FEI Quanta 200 scanning electron microscope (SEM) equipped with an X-ray spectroscope. The energy-dispersive spectrometry (EDS) elemental analyses on several single crystals for the two compounds gave average Rb/I/O and Rb/I/O/F molar ratios of approximately 0.9:1:3 and 1.1:1:2.4:2 for RbIO₃ and RbIO₂F₂, which is in good agreement with those determined from single-crystal X-ray structure analyses (Figure S5 and S6).

Infrared Spectrum and UV–vis Diffuse Reflectance Spectrum. The IR spectra were carried out on a NICOLET 5700 Fourier-transformed infrared (FTIR) spectrophotometer in the 4000–700 cm⁻¹ region (2.5–14 μm) using the attenuated total reflection (ATR) technique with a germanium crystal. The UV–vis diffuse reflectance spectra were performed on a Varian Cary 5000 UV–vis–NIR spectrophotometer in the region 200–800 nm. A BaSO₄ plate was

Table 1. Crystallographic Data for RbIO₃ and RbIO₂F₂

formula	RbIO ₃	RbIO ₂ F ₂
FW	260.37	282.37
T (K)	296(2)	298(2)
wavelength (Å)	0.71073	0.71073
crystal color	colorless	colorless
space group	R3m	Pca21
a (Å)	6.413(2)	8.567(4)
b (Å)	6.413(2)	6.151(3)
c (Å)	7.854(2)	8.652(4)
α (deg)	90	90
β (deg)	90	90
γ (deg)	120.00	90
volume (Å ³)	279.73(14)	455.9(4)
Z	3	4
dcacl (g cm ⁻³)	4.637	4.114
F(000)	342	496
reflections collected	748	4416
independent reflections	226	1350
R1, wR2 [I > 2σ(I)]	0.0730/0.1923	0.0215/0.0492
R1, wR2 (all data)	0.0730/0.1923	0.0229/0.0500
min/max Δρ/eÅ ⁻³	−5.632/5.059	−0.823/0.786

used as the standard (100% reflectance), on which the finely ground samples from the crystals were coated. The absorption spectrum was calculated from reflectance spectrum using the Kubelka–Munk function:³⁷ $\alpha/S = (1 - R)^2/2R$, where α is the absorption coefficient, S is the scattering coefficient, and R is the reflectance.

NLO Property and LDT Measurement. Powder second-harmonic generation (SHG) signals were measured using the method adapted from Kurtz and Perry.³⁸ A pulsed Q-switched Nd:YAG laser was utilized to generate fundamental 1064 nm light with a pulse width of 10 ns. The samples were pressed between two glasses. To make relevant comparisons with known SHG materials, microcrystalline KH₂PO₄ (KDP) served as the standard. The powders RbIO₃, RbIO₂F₂, and KDP were ground and sieved into the same particle size (100–125 μm). Since phase-matchable SHG materials are very important owing to their applications, we searched for the relationships between SHG efficiencies and particle sizes. Polycrystalline samples were ground and sieved into the following particle size ranges: 20–40, 40–60, 60–80, 80–100, 100–125, 125–150, 150–200, 200–300, 300–400, and 400–500 μm. The laser-induced damage threshold (LDT) tests were performed on powder samples which were obtained by grinding the single crystal, with the laser source (1064 nm, 5 ns, 1 Hz). The two compounds and AgGaS₂ were ground and sieved into the same particle size range (100–200 μm). The energy of the laser emission was gradually increased until the color of the samples changed.^{10–12} It should be noted that the LDT measurement using powder samples is feasible since each crystallite has a diameter much larger than the wavelength of the incident laser. Thus, each crystallite behaves as a macroscopic bulk material with the similar multiphoton absorption (a main process for LDT as the laser pulse width is shorter than 50 ps).³⁹

Thermogravimetric Analysis. The thermogravimetric analysis (TGA) was carried out with a Netzsch STA 449c analyzer instrument. Crystal samples were added into an Al₂O₃ crucible and heated from room temperature to 800 °C at a rate of 10 K/min under flowing nitrogen gas.

Computational Methods. The first-principles calculations at the atomic level for the RbIO₃ and RbIO₂F₂ crystals were performed by the plane-wave pseudopotential method⁴⁰ implemented in the CASTEP program⁴¹ based on density functional theory (DFT).⁴² The exchange–correlation (XC) functionals were described by the local density approximation (LDA).⁴³ The ion–electron interactions were modeled by the ultrasoft pseudopotentials⁴⁴ for all constituent elements. In this model, Rb 4s²4p⁶5s¹, O 2s²2p⁴, I 5s²5p⁵, and F 2s²2p⁵ are treated as the valence electrons, respectively. A kinetic energy

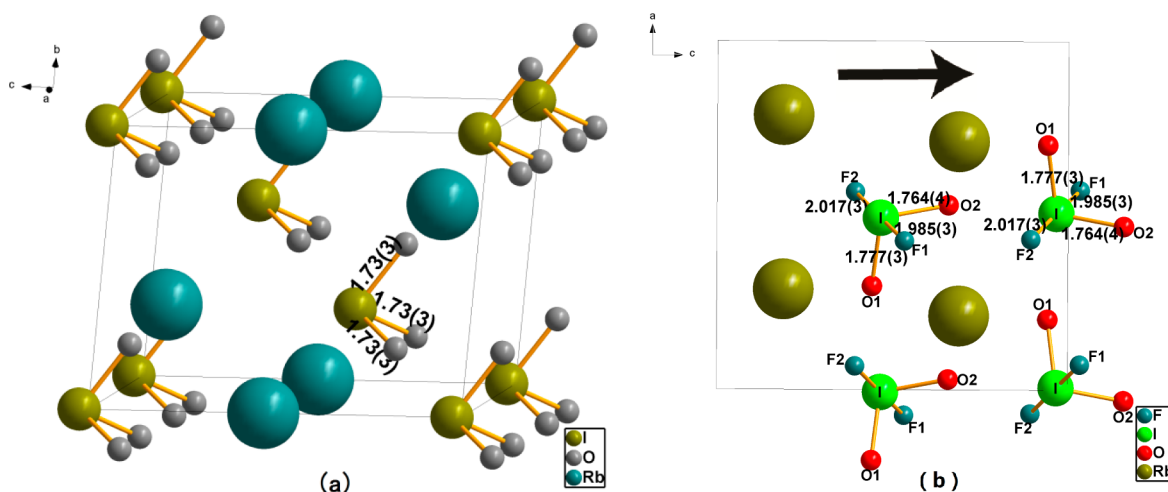


Figure 1. (a) Ball-and-stick diagrams of RbIO_3 . (b) Ball-and-stick diagrams of RbIO_2F_2 .

cutoff of 400 eV and Monkhorst–Pack k -point meshes⁴⁵ spanning less than $0.04/\text{\AA}^3$ in the Brillouin zone were chosen to ensure the sufficient accuracy of the present purposes.

RESULTS AND DISCUSSION

Synthesis Method. In this work, RbIO_3 was synthesized by a hydrothermal reaction which is different from the solution method in the literature.⁴⁶ RbIO_2F_2 is a new compound, and we also used a hydrothermal synthetic method for its preparation, mainly in the hope to get larger size crystalline product directly in hydrothermal reaction.

Crystal Structure. The crystal structure of RbIO_3 determined in this work is essentially the same as that reported in the literature,³⁰ and the cell parameters are similar. RbIO_3 crystallizes in the acentric space group $R3m$. Its structure is very simple. It contains I^{5+} cation with a lone pair of electrons. Figure 1a clearly shows that each I atom is coordinated with three O atoms to form a distorted trigonal-pyramidal environment $[\text{IO}_3]^-$. All the I–O bond lengths in the $[\text{IO}_3]^-$ anion group are the same (1.73(3) Å). All the $[\text{IO}_3]^-$ anion groups are arranged in the same direction. It is such arrangement that results in a macroscopic net polarization leading to large SHG responses. On the other hand, RbIO_2F_2 crystallizes in the acentric space group $Pca21$. It also contains I^{5+} cation with a lone pair of electrons. From Figure 1b, one may see that each I atom is linked to two O atoms and two F atoms to form a distorted tetrahedron anion group $[\text{IO}_2\text{F}_2]^-$. Two I–F bond lengths (1.985(3) and 2.017(3) Å) are longer than two I–O lengths (1.764(4) and 1.777(3) Å). The F2–I–F1 bond angle is almost 180° ($177.79(13)^\circ$), and thus, the dipole moments of I–F1 and I–F2 nearly cancel each other. Analogously, a half number of O1–I bonds are almost parallel to the a -axis, whereas the other half of O1–I bonds are almost antiparallel to the a -axis; therefore, all O1–I bonds together contribute almost nothing to the net dipole moment in the $[\text{IO}_2\text{F}_2]^-$ group. In comparison, all O2–I bonds are almost parallel to the c -axis, and the result is a net dipole moment in the whole crystal structure along this direction (see black arrow in Figure 1b). This net polarization leads to a moderate SHG response in RbIO_2F_2 .

Infrared Spectrum and UV–vis Diffuse Reflectance Spectrum. The IR spectra of RbIO_3 and RbIO_2F_2 exhibit wide transparent range from 2.5 to 13.6 (4000 – 735 cm^{-1}) and 2.5– $12.3\text{ }\mu\text{m}$ (4000 – 810 cm^{-1}), respectively (Figure 2). These

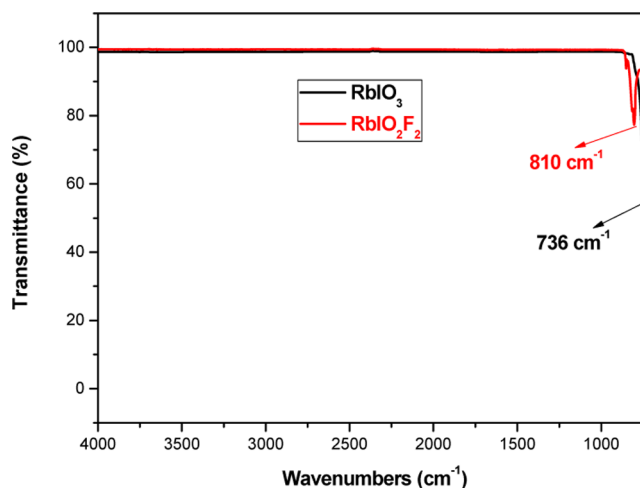


Figure 2. FTIR spectra for RbIO_3 and RbIO_2F_2 (4000 – 700 cm^{-1} region).

results are consistent with the IR absorption data for other metallic iodate NLO materials.^{10,17,47} Although there would have some deviation from the measurement on single crystals, the IR absorption edge of powder samples can at least provide the preliminary evidence to determine the transparent region of materials. Our measured data clearly indicate that both RbIO_3 and RbIO_2F_2 are transparent in the mid-IR region from 3 to $5\text{ }\mu\text{m}$. The UV–vis diffuse reflectance spectra of RbIO_3 and RbIO_2F_2 show that the absorption edge in the UV side is about 310 and 295 nm, indicating that the band gaps of two compounds can be calculated to be 4.0 and 4.2 eV (Figure 3), respectively. The result is consistent with our design strategy that introducing F^- into RbIO_3 can expand the band gap so as to improve the LDT.

Thermogravimetric Analysis. The TGA curves for the RbIO_3 and RbIO_2F_2 powders in nitrogen are shown in Figure 4. It is clear that both compounds have a relatively high thermal stability. RbIO_3 is stable up to $550\text{ }^\circ\text{C}$, and RbIO_2F_2 is $400\text{ }^\circ\text{C}$.

NLO Properties and LDT Measurements. Powder SHG measurements using 1064 nm laser revealed that RbIO_3 and RbIO_2F_2 powders exhibit SHG effects of about 20 and 4 times that of KDP (at the same particle size range of 100 – $125\text{ }\mu\text{m}$). The result that the SHG effect of RbIO_2F_2 is much weaker than that of RbIO_3 may come from the following reasons: First, the

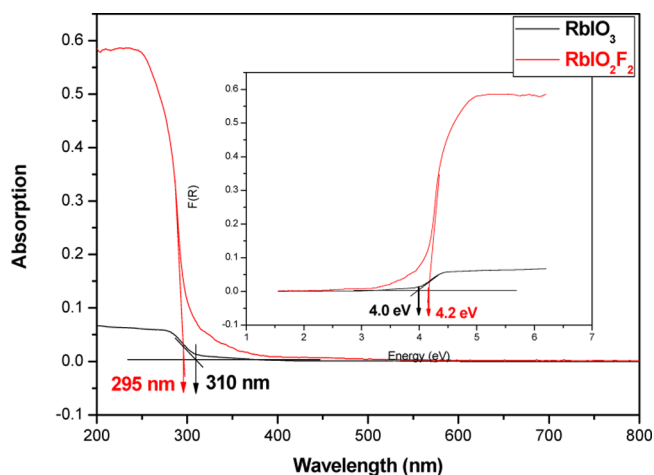


Figure 3. UV-vis absorption spectra for RbIO_3 and RbIO_2F_2 .

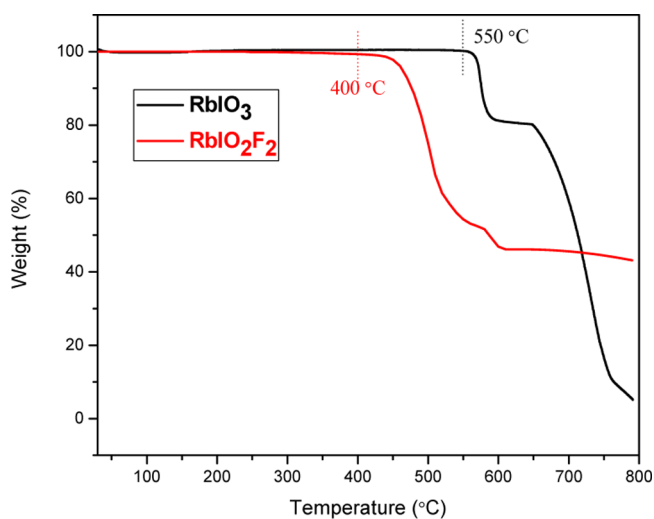


Figure 4. Thermogravimetric analysis curves for RbIO_3 and RbIO_2F_2 .

electronic negativity of F is stronger than that of O so the electronic clouds on the $[\text{IO}_2\text{F}_2]^-$ anionic groups are less polarizable than those on the $[\text{IO}_3]^-$ groups. Second, the $[\text{IO}_3]^-$ groups form trigonal-pyramids with strong dipolarity, while the $[\text{IO}_2\text{F}_2]^-$ groups form distorted tetrahedrons with smaller dipolarity. Third, all the $[\text{IO}_3]^-$ groups in the crystal of RbIO_3 are arranged in a perfectly parallel direction (see Figure 1a), giving rise to a large net dipolarity, whereas in the crystal structure of RbIO_2F_2 (see Figure 1b), the arrangement of the $[\text{IO}_2\text{F}_2]^-$ groups is far less perfectly parallel than that of $[\text{IO}_3]^-$ groups in RbIO_3 , resulting in a much smaller net dipolarity. As shown in Figure 5, for two compounds, the powder SHG intensities at first increase gradually with the increase in particle size and then reach a plateau. This is a typical curve of the phase-matchable materials. It is an important factor for the materials to be practically useful. Following the method in the literature,¹⁰ a preliminary measurement of the LDT has been performed on powders with the AgGaS_2 powders as the reference at the same measurement conditions. Table 2 lists the LDT values for RbIO_3 , RbIO_2F_2 and some representative mid-IR NLO compounds (measured in the same condition). The results show that the LDT values of the AgGaS_2 , KIO_3 , $\text{K}_2\text{BiI}_5\text{O}_{15}$, and $\text{Rb}_2\text{BiI}_5\text{O}_{15}$ powders are 5.2, 140, 84, and 72 MW/cm^2 , respectively, while the values for the titled

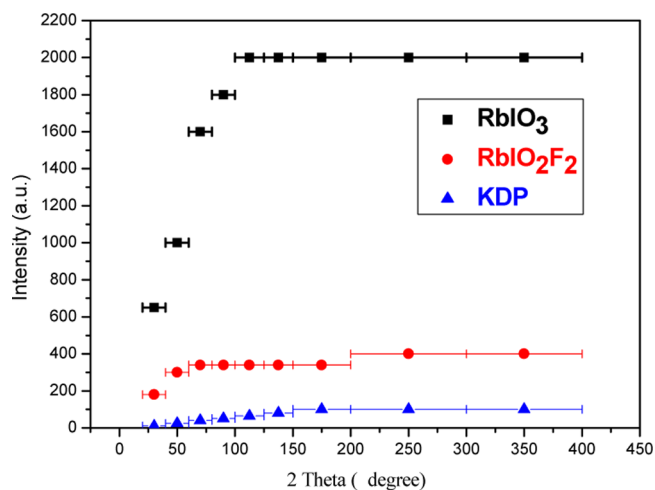


Figure 5. Dependence of SHG intensity on the particle size of RbIO_3 , RbIO_2F_2 , and KDP, respectively.

Table 2. LDT Values for RbIO_3 , RbIO_2F_2 , and Some Representative Mid-IR NLO Compounds (Measured in the Same Condition)

	AgGaS_2	KIO_3	$\text{K}_2\text{BiI}_5\text{O}_{15}$	$\text{Rb}_2\text{BiI}_5\text{O}_{15}$	RbIO_3	RbIO_2F_2
LDT (MW/cm^2)	5	140	84	72	125	156

compounds are 125 MW/cm^2 (RbIO_3) and 156 MW/cm^2 (RbIO_2F_2), indicating that both RbIO_3 and RbIO_2F_2 show much higher LDT than AgGaS_2 . In particular, the LDT of RbIO_2F_2 is higher than RbIO_3 , KIO_3 , $\text{K}_2\text{BiI}_5\text{O}_{15}$, and $\text{Rb}_2\text{BiI}_5\text{O}_{15}$. Because the above values obtained on the powders are underestimated, the value on the single crystal should be higher. The result that the LDT value of RbIO_2F_2 is higher than that of RbIO_3 is in good agreement with our design strategy by partially replacing O^{2-} of RbIO_3 with F^- to improve LDT. The more accurate LDT and IR absorption measurements on RbIO_3 and RbIO_2F_2 will be made as the single crystals with large size and good quality are obtained in the future studies.

Theoretical Results. The first-principles partial density of states (PDOS) projected on the constitutional atoms were plotted in Figure 6a,b, respectively, for RbIO_3 and RbIO_2F_2 . Note that the top of the valence band (VB) and the bottom of conduction band (CB) are mainly occupied by the orbitals of O (2p), I (5p), and F (2p). Namely, the states on both sides of the band gap are mainly composed of the orbitals from the $(\text{IO}_3)^-$ and $(\text{IO}_2\text{F}_2)^-$ groups in RbIO_3 and RbIO_2F_2 . Since the optical response of a crystal in the visible-IR region originates mainly from the electronic transitions between the VB and CB states close to the band gap,⁴⁸ the $(\text{IO}_3)^-$ or $(\text{IO}_2\text{F}_2)^-$ anionic units are considered to mainly determine the optical properties of the crystal series. Moreover, in RbIO_2F_2 , the energy spanning of F 2p orbitals is about 5 eV at the top of VB, and they exhibit quite large hybridization with the orbitals on the neighbor ions. This decreases the energy bandwidth of the VB and enlarges the energy band gap in RbIO_2F_2 . Therefore, the absorption edge of RbIO_2F_2 is blue-shifted compared with RbIO_3 , which is also confirmed by the first-principles band gaps for these two compounds (4.2 eV for RbIO_2F_2 vs 2.8 eV for RbIO_3). In fact, the enlargement of band gap by incorporation of fluorine has been observed in UV NLO crystals⁴⁹ but is directly demonstrated in the mid-IR NLO materials for the first time

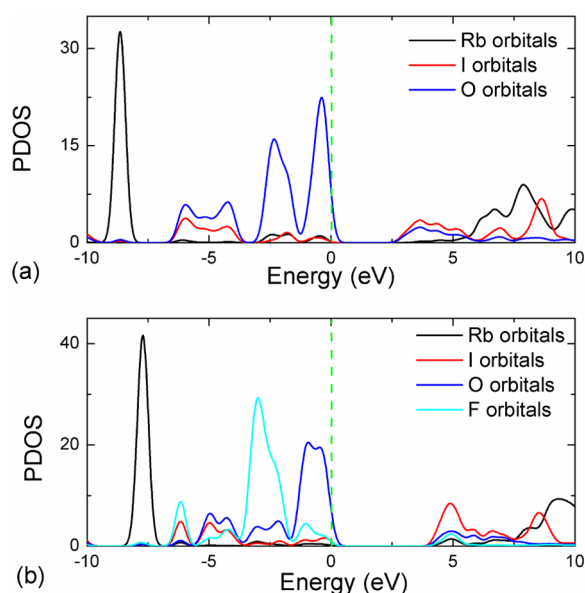


Figure 6. Partial density of states (PDOS) of RbIO₃ (a) and RbIO₂F₂ (b).

in this study. Moreover, it is well-known that energy bandgaps determine the multiphoton absorption processes, and a larger bandgap usually corresponds to a larger LDT in the crystal. The much larger bandgap of RbIO₂F₂ (>4 eV) than that of AgGaS₂ (~2.6 eV) confirms the conclusion obtained from the powder LDT measures.

Based on the obtained electronic structure, the SHG coefficients (d_{ij}) of the two crystals are computed by the scissors-corrected LDA approach,^{50,51} and the corresponding powder-SHG (PSHG, $\langle d_{\text{powder}} \rangle$) effects are obtained according to the Kurtz–Perry method, which are listed in Table S7. PSHG effects are 8.5 and 5.5 times larger than that of KDP ($\langle d_{\text{powder}} \rangle = 0.33$ pm/V) for RbIO₃ and RbIO₂F₂, respectively, consistent with those of experimental measurements (20 and 4 times KDP, respectively). In addition, the calculated birefringence values for both compounds are moderate (~0.06), which indicates that their phase-matching capability for second-order generation in the mid-IR region can be achieved.

CONCLUSION

A halogenated oxysalt RbIO₃ is synthesized in hydrothermal reaction and then systematically evaluated for its potential as a new NLO material in the mid-IR region. Its powders show strong SHG responses (20 times KDP), high LDT (125 MW/cm², about 20 times higher than that of AgGaS₂ powders measured in the same condition), wide transparent region (0.3–13 μm), and high thermal stability (550 °C). By introducing F⁻ anion into RbIO₃, we successfully obtained a new material RbIO₂F₂, which exhibits an even higher LDT value (156 MW/cm²) than that of RbIO₃, while exhibiting good SHG effect (4 times KDP), wide transparent region (0.3–12 μm), and high thermal stability (400 °C). All the results indicate that both RbIO₃ and RbIO₂F₂ are promising NLO materials in mid-IR region from 3 to 5 μm. Moreover, this work may open a new way for searching for new mid-IR NLO materials with higher laser damage threshold and good comprehensive properties by partially replacing an anion

(such as O²⁻ anion in a known oxysalt NLO material) with another anion of stronger electronegativity (such as F⁻).

ASSOCIATED CONTENT

Supporting Information

The Supporting Information is available free of charge on the ACS Publications website at DOI: 10.1021/acs.chemmater.5b04511.

Photograph of the single crystal of RbIO₃ and RbIO₂F₂, powder X-ray diffraction pattern data, EDX spectrum, atomic coordinates and equivalent isotropic displacement parameters and some selected important bond lengths and angles, the calculated linear and nonlinear optical properties and CIF files (PDF)

AUTHOR INFORMATION

Corresponding Authors

*E-mail: jgqin@whu.edu.cn.

*E-mail: zslin@mail.ipc.ac.cn.

Notes

The authors declare no competing financial interest.

ACKNOWLEDGMENTS

This work was financially supported by the National Basic Research Program of China (No. 2010CB630701), the Natural Science Foundation of China. (No. 91022036) and the 863 Program of China (No. 2015AA034203).

REFERENCES

- Burland, D. M.; Miller, R. D.; Walsh, C. A. Second-order nonlinearity in poled-polymer systems[J]. *Chem. Rev.* **1994**, *94*, 31–75.
- Chemla, D. S.; Kupecek, P. J.; Robertson, D. S.; Smith, R. C. Silver thiogallate, a new material with potential for infrared devices. *Opt. Commun.* **1971**, *3*, 29–31.
- Boyd, G. D.; Kasper, H. M.; McFee, J. H.; Storz, F. G. Linear and Nonlinear Optical Properties of some ternary selenides. *IEEE J. Quantum Electron.* **1972**, *8*, 900–908.
- Boyd, G. D.; Buehler, E.; Storz, F. G. Linear and Nonlinear Optical Properties of ZnGeP₂ and CdSe. *Appl. Phys. Lett.* **1971**, *18*, 301–304.
- Kang, L.; Zhou, M.; Yao, J.; Lin, Z.; Wu, Y.; Chen, C. metal thiophosphates with good mid infrared nonlinear optical performances: a first-principles prediction and analysis. *J. Am. Chem. Soc.* **2015**, *137*, 13049–13059.
- Lin, X.; Zhang, G.; Ye, N. Growth and Characterization of BaGa₄S₇: A New Crystal for Mid-IR Nonlinear Optics. *Cryst. Growth Des.* **2009**, *9*, 1186–1189.
- Mei, D.; Yin, W.; Bai, L.; Lin, Z.; Yao, J.; Fu, P.; Wu, Y. BaAl₄Se₇: a new infrared nonlinear optical material with a large band gap. *Dalton Trans.* **2011**, *40*, 3610–3615.
- Isaenko, L.; Vasilyeva, I. G. Nonlinear LiB^{III}C^{VI}₂ crystals for mid-IR and far-IR: Novel aspects in crystal growth. *J. Cryst. Growth* **2008**, *310*, 1954–1960.
- Ra, H. S.; Ok, K. M.; Halasyamani, P. S. Combining Second-Order Jahn-Teller Distorted Cations to Create Highly Efficient SHG Materials: Synthesis, Characterization, and NLO Properties of BaTeM₂O₉ (M = Mo⁶⁺ or W⁶⁺). *J. Am. Chem. Soc.* **2003**, *125*, 7764–7765.
- Phanon, D.; Gautier-Luneau, I. Promising Material for Infrared Nonlinear Optics: NaI₃O₈ Salt Containing an Octaoxotriiodate(V) Anion Formed from Condensation of [IO₃]⁻ Ions. *Angew. Chem., Int. Ed.* **2007**, *46*, 8488–8491.
- Zhang, M.; Li, B.; Liu, B.; Fan, Y.; Li, X.; Zeng, H.; Guo, G. Ln₃GaS₆ (Ln = Dy, Y): new infrared nonlinear optical materials with

high laser induced damage thresholds. *Dalton Trans.* **2013**, 42, 14223–14229.

(12) Zhang, M.; Jiang, X.; Zhou, L.; Guo, G. Two phases of Ga_2S_3 : promising infrared second-order nonlinear optical materials with very high laser induced damage thresholds. *J. Mater. Chem. C* **2013**, 1, 4754–4760.

(13) Nguyen, S. D.; Yeon, J.; Kim, S. H.; Halasyamani, P. S. $\text{BiO}(\text{IO}_3)$: A New Polar Iodate that Exhibits an Aurivillius-Type $(\text{Bi}_2\text{O}_2)^{2+}$ Layer and a Large SHG Response. *J. Am. Chem. Soc.* **2011**, 133, 12422–12425.

(14) Xu, X.; Hu, C.; Li, B.; Yang, B.; Mao, J. $\alpha\text{-AgI}_3\text{O}_8$, $\beta\text{-AgI}_3\text{O}_8$ with Large SHG Responses: Polymerization of IO_3 Groups into the I_3O_8 Polyiodate Anion. *Chem. Mater.* **2014**, 26, 3219–3230.

(15) Zhang, G.; Li, Y.; Zeng, H.; Liu, T.; Chen, X.; Qin, J.; Lin, Z.; Fu, P.; Wu, Y.; Chen, C. A New Mixed-halide, $\text{Cs}_2\text{HgI}_2\text{Cl}_2$: Molecular Engineering for New Nonlinear Optical Material in the IR Region. *J. Am. Chem. Soc.* **2012**, 134, 14818–14822.

(16) Wu, Q.; Meng, X.; Zhong, C.; Chen, X.; Qin, J. $\text{Rb}_2\text{CdBr}_2\text{I}_2$: A New IR Nonlinear Optical Material with a Large Laser Damage Threshold. *J. Am. Chem. Soc.* **2014**, 136, 5683–5686.

(17) Cao, Z.; Yue, Y.; Yao, J.; Lin, Z.; He, R.; Hu, Z. $\text{Bi}_2(\text{IO}_4)(\text{IO}_3)_3$: A New Potential Infrared Nonlinear Optical Material Containing $[\text{IO}_4]^{3-}$ Anion. *Inorg. Chem.* **2011**, 50, 12818.

(18) Huang, Y.; Meng, X.; Gong, P.; Yang, L.; Lin, Z.; Chen, X.; Qin, J. $\text{A}_2\text{BiI}_5\text{O}_{15}$ ($\text{A} = \text{K}^+$ or Rb^+): two new promising nonlinear optical materials containing $[\text{I}_3\text{O}_9]^{3-}$ bridging anionic groups. *J. Mater. Chem. C* **2014**, 2, 4057–4062.

(19) Chang, H.; Kim, S. H.; Halasyamani, P. S.; Ok, K. M. Alignment of Lone Pairs in a New Polar Material: Synthesis, Characterization, and Functional Properties of $\text{Li}_2\text{Ti}(\text{IO}_3)_6$. *J. Am. Chem. Soc.* **2009**, 131, 2426–2427.

(20) Chang, H.; Kim, S. H.; Ok, K. M.; Halasyamani, P. S. Polar or Nonpolar? A^+ Cation Polarity Control in $\text{A}_2\text{Ti}(\text{IO}_3)_6$ ($\text{A} = \text{Li}, \text{Na}, \text{K}, \text{Rb}, \text{Cs}, \text{Tl}$). *J. Am. Chem. Soc.* **2009**, 131, 6865–6873.

(21) Sykora, R. E.; Ok, K. M.; Halasyamani, P. S.; Wells, D. M.; Albrecht-Schmitt, T. E. New one-dimensional vanadyl iodates: Hydrothermal Preparation, Structures and NLO properties of $\text{A}[\text{VO}_2(\text{IO}_3)_2]$ ($\text{A} = \text{K}, \text{Rb}$) and $\text{A}[(\text{VO})_2(\text{IO}_3)_3\text{O}_2]$ ($\text{A} = \text{NH}_4^+, \text{Rb}, \text{Cs}$). *Chem. Mater.* **2002**, 14, 2741–2749.

(22) Sun, C.; Hu, C.; Xu, X.; Yang, B.; Mao, J. Explorations of New Second-Order Nonlinear Optical Materials in the Potassium Vanadyl Iodate System. *J. Am. Chem. Soc.* **2011**, 133, 5561–5572.

(23) Huang, C.; Hu, C.; Xu, X.; Yang, B.; Mao, J. $\text{Tl}(\text{VO})_2\text{O}_2(\text{IO}_3)_3$: a new polar material with a strong SHG response. *Dalton Trans.* **2013**, 42, 7051–7058.

(24) Sun, C.; Hu, C.; Xu, X.; Ling, J.; Hu, T.; Kong, F.; Long, X.; Mao, J. $\text{BaNbO}(\text{IO}_3)_5$: A New Polar Material with a Very Large SHG Response. *J. Am. Chem. Soc.* **2009**, 131, 9486–9487.

(25) Chen, X.; Zhang, L.; Chang, X.; Xue, H.; Zang, H.; Xiao, W.; Song, X.; Yan, H. $\text{LiMoO}_3(\text{IO}_3)$: A new molybdenyl iodate based on WO_3 type sheets with large SHG response. *J. Alloys Compd.* **2007**, 428, 54–58.

(26) Sykora, R. E.; Ok, K. M.; Halasyamani, P. S.; Albrecht-Schmitt, T. E. Structural Modulation of Molybdenyl Iodate Architectures by Alkali Metal Cations in $\text{AMoO}_3(\text{IO}_3)$ ($\text{A} = \text{K}, \text{Rb}, \text{Cs}$): A Facile Route to New Polar Materials with Large SHG Responses. *J. Am. Chem. Soc.* **2002**, 124, 1951–1957.

(27) Sun, C.; Hu, C.; Xu, X.; Mao, J. Polar or Non-Polar? Syntheses, Crystal Structures, and Optical Properties of Three New Palladium (II) Iodates. *Inorg. Chem.* **2010**, 49, 9581–9589.

(28) OK, K. M.; Halasyamani, P. S. New Metal Iodates: Syntheses, Structures, and Characterizations of Noncentrosymmetric $\text{La}(\text{IO}_3)_3$ and $\text{NaYI}_4\text{O}_{12}$ and Centrosymmetric $\beta\text{-Cs}_2\text{I}_4\text{O}_{11}$ and $\text{Rb}_2\text{I}_6\text{O}_{15}(\text{OH})_2 \cdot \text{H}_2\text{O}$. *Inorg. Chem.* **2005**, 44, 9353–9359.

(29) Hu, C.; Mao, J. Recent advances on second-order NLO materials based on metal iodates. *Coord. Chem. Rev.* **2015**, 288, 1–17.

(30) Dmitriev, V. G.; Gurzadyan, G. G.; Nikogosyan, D. N. In *Handbook of Nonlinear Optical Crystals (Springer Series in Optical Sciences)*, Vol.64; Siegmán, A. E., Ed.; Springer Verlag, 1991.

(31) Belokoneva, E. L.; Stefanovich, S. Y.; Dimitrova, O. V. New nonlinear optical potassium iodate $\text{K}[\text{IO}_3]$ and borates $\text{K}_3[\text{B}_6\text{O}_{10}]\text{Br}$, $\text{KTa}[\text{B}_4\text{O}_6(\text{OH})_4](\text{OH})_2 \cdot 1.33\text{H}_2\text{O}$: Synthesis, structures and relation to the properties. *J. Solid State Chem.* **2012**, 195, 79–85.

(32) Alcock, N. W. Crystal structure of α -rubidium iodate. *Acta Crystallogr., Sect. B: Struct. Crystallogr. Cryst. Chem.* **1972**, 28, 2783–2788.

(33) Kurtz, S. K.; Perry, T. T.; Bergman, J. G., Jr. Alpha-iodic acid: a solution-grown crystal for nonlinear optical studies and applications. *Appl. Phys. Lett.* **1968**, 12, 186–188.

(34) Xu, X.; Yang, B.; Huang, C.; Mao, J. Explorations of New Second-Order Nonlinear Optical Materials in the Ternary Rubidium Iodate System: Noncentrosymmetric $\beta\text{-RbIO}_3(\text{HIO}_3)_2$ and Centrosymmetric $\text{Rb}_3(\text{IO}_3)_3(\text{I}_2\text{O}_5)$ (HIO_3) $_4(\text{H}_2\text{O})$. *Inorg. Chem.* **2014**, 53, 1756–1763.

(35) Sheldrick, G. M. *SHELXTL*, version 6.14; Bruker Analytical Xray Instruments, Inc.: Madison, WI, 2003.

(36) Sheldrick, G. M. A short history of SHELX. *Acta Crystallogr., Sect. A: Found. Crystallogr.* **2008**, A64, 112.

(37) Wendlandt, W. W.; Hecht, H. G. *Reflectance Spectroscopy*; Interscience: New York, 1966; pp 62–65.

(38) Kurtz, S. K.; Perry, T. T. A Powder Technique for the Evaluation of Nonlinear Optical Materials. *J. Appl. Phys.* **1968**, 39, 3798–3812.

(39) Brant, J. A.; Clark, D. J.; Kim, Y. S.; Jang, J. I.; Weiland, A.; Aitken, J. A. Outstanding Laser Damage Threshold in $\text{Li}_2\text{MnGeS}_4$ and Tunable Optical Nonlinearity in Diamond-Like Semiconductors. *Inorg. Chem.* **2015**, 54, 2809–2819.

(40) Payne, M. C.; Teter, M. P.; Allan, D. C.; Arias, T. A.; Joannopoulos, J. D. Iterative minimization techniques for ab initio total-energy calculations: molecular dynamics and conjugate gradients. *Rev. Mod. Phys.* **1992**, 64, 1045–1097.

(41) Clark, S. J.; Segall, M. D.; Pickard, C. J.; Hasnip, P. J.; Probert, M. J.; Refson, K.; Payne, M. C. First principles methods using CASTEP. *Z. Kristallogr. - Cryst. Mater.* **2005**, 220, 567–570.

(42) Kohn, W. Nobel Lecture: Electronic structure of matter-wave functions and density functionals [J]. *Rev. Mod. Phys.* **1999**, 71, 1253–1266.

(43) Ceperley, D. M.; Alder, B. J. Ground-State of The Electron-gas by a stochastic method [J]. *Phys. Rev. Lett.* **1980**, 45, 566–569.

(44) Lin, J.; Qteish, A.; Payne, M. C.; Heine, V. Optimized and transferable nonlocal separable abinitio pseudopotentials [J]. *Phys. Rev. B: Condens. Matter Phys.* **1993**, 47, 4174–4180.

(45) Monkhorst, H. J.; Pack, J. D. Special points for brillouin-zone integrations [J]. *Phys. Rev. B* **1976**, 13, 5188–5192.

(46) Shklovskaya, R. M.; Vulikh, A. I. High-purity rubidium and cesium chlorates, bromates, and iodates. *Methods for Synthesis of Chemical Reagents and Preparations* **1967**, 16, 77–84.

(47) Phanon, D.; Mosset, A.; Gautier-Luneau, I. New materials for infrared non-linear optics. Syntheses, structural characterisations, second harmonic generation and optical transparency of $\text{M}(\text{IO}_3)_3$ metallic iodates. *J. Mater. Chem.* **2007**, 17, 1123–1130.

(48) Lee, M. H.; Yang, C.; Jan, J. Band-resolved analysis of nonlinear optical properties of crystalline and molecular materials [J]. *Phys. Rev. B: Condens. Matter Phys.* **2004**, 70, 235110.

(49) Zhao, S.; Gong, P.; Luo, S.; Bai, L.; Lin, Z.; Tang, Y.; Zhou, Y.; Hong, M.; Luo, J. Tailored Synthesis of a Nonlinear Optical Phosphate with a Short Absorption Edge. *Angew. Chem., Int. Ed.* **2015**, 54, 4217–4221.

(50) Wang, C.; Klein, B. M. 1st-principles Electronic structure of SI , GE , GAP , GAAS , ZNS , and ZNSE 0.1. Self-consistent energy-bands, charge-densities, and Effective masses [J]. *Phys. Rev. B: Condens. Matter Phys.* **1981**, 24, 3393–3416.

(51) Godby, R. W.; Schluter, M.; Sham, L. J. Self-energy operators and exchange-correlation potentials in semiconductors [J]. *Phys. Rev. B: Condens. Matter Phys.* **1988**, 37, 10159–10175.